Analysis of Ultrasonic 3-D Image Compression Using Non-Uniform, Separable Wavelet Transforms

Erdal Oruklu, Sonali Maharishi and Jafar Saniie
Department of Electrical and Computer Engineering
Illinois Institute of Technology
Chicago, Illinois, 60616

***Abstract*—In this study, we analyze efficient volumetric ultrasonic data compression algorithms which require fewer computations and can be implemented with fewer hardware resources. Discrete Wavelet Transform (DWT) is used for compression of 3-D ultrasound data. Different wavelet kernels are analyzed and benchmarked for compression of experimental signals. In order to reduce computational complexity, non-uniform DWT method is utilized where different wavelet filters are applied to ultrasonic axial resolution and spatial resolutions. Axial resolution contains more information than spatial resolutions; therefore simple wavelet filters such as Haar can be used for the spatial resolutions reducing the computations significantly.**

I. Introduction

Data compression is essential for applications where distributed sensor networks are used and large amount of data are shared between platforms with limited communication bandwidth. These applications may involve ultrasonic, sonar or radar signals/images and besides high compression ratios, they require the reduced bandwidth output (i.e., reconstructed image or signal from compressed data) to be virtually indistinguishable from the original. Although existing photographic image compression methods are applicable, these methods are not optimal.

In the past, several well-known compression methods and standards such as Joint Photographic Experts Group (JPEG), Embedded Zero-Tree Wavelets (EZW) [1], Set Partitioning in Hierarchical Tree (SPIHT) [2], and JPEG2000 [3] have been applied to ultrasonic data compression with mixed results. These methods have been developed primarily for photographic images without taking into account the ultrasound signal properties where data is acquired through a pulse-echo system. In conventional ultrasound systems, the radio-frequency (RF) data obtained after the analog-to-digital (A/D) converter are passed through an envelope detector, and then decomposed and processed to form the ultrasound image. However, all the information about the spectral content of the signal external to the range of interest are lost. Furthermore, an ultrasound image also has a significant variation in pixel statistics across a single image which presents a challenge to existing coding methods. These lead to suboptimal compression ratios as well as image fidelity issues.

We address these challenges by examining the RF signal directly. In this study, Discrete Wavelet Transform (DWT) is used for compression of 3-D ultrasound data and different wavelet kernels are analyzed and benchmarked. DWT has been used for ultrasonic compression applications due to its high energy compaction properties. In particular, optimal wavelet kernel design has been presented for ultrasonic compression in [4]. Parameter estimation techniques have been studied in [5] and DWT has been compared to other transform based compression methods in [6]. A major challenge for embedded device implementations is the large computational requirements for DWT operation in three separate dimensions (especially if the wavelet filter employed is high order). In order to reduce computational complexity, non-uniform DWT method [7], [8] is utilized where different wavelet filters are applied to ultrasonic axial resolution and spatial resolutions. This way better compression results can be achieved by exploring resolution characteristics in different directions of ultrasound images, and the processing time decreases significantly.

The paper is organized as follows. Section II describes the wavelet transform and ultrasonic compression methods. Section III presents the non-uniform 3-D wavelet transform. The compression algorithm, including the thresholding techniques and different wavelet kernels are described in section IV. The experimental setup and results are detailed in Section V, and the conclusion is given in Section VI.

II. Wavelet Transform

The forward DWT can be represented in matrix form as

$$X = [W]x \tag{1}$$

where the NXN real-valued kernel matrix $[W]$ defines the DWT. The DWT is a unitary and orthonormal transform, hence, $WW^T = I$ and $\|X(m)\|^2 = \|x(n)\|^2$. The matrix $[W]$ is built by shifts and dilations of the wavelet kernel. An important advantage of the DWT over other transforms is that the wavelet kernel is not restricted to a set of functions (e.g. cosines in the DCT case). In principle, the number of different wavelet kernels is unlimited. Any function that satisfies the admissibility conditions is a wavelet kernel.

The implementation of the wavelet transform requires a perfect reconstruction filter bank. Fig. 1 shows an example of the wavelet filter bank applied to a 1-D signal, $x(n)$, where low pass (H_0) and high pass (H_1) filters are used for the forward DWT operation. The filterbank operations can be repeated for multi-level wavelet decomposition. At each level of decomposition, the signal frequency spectrum is split. The transformed signal has both spatial and frequency

1051-0117/07/$25.00 ©2007 IEEE

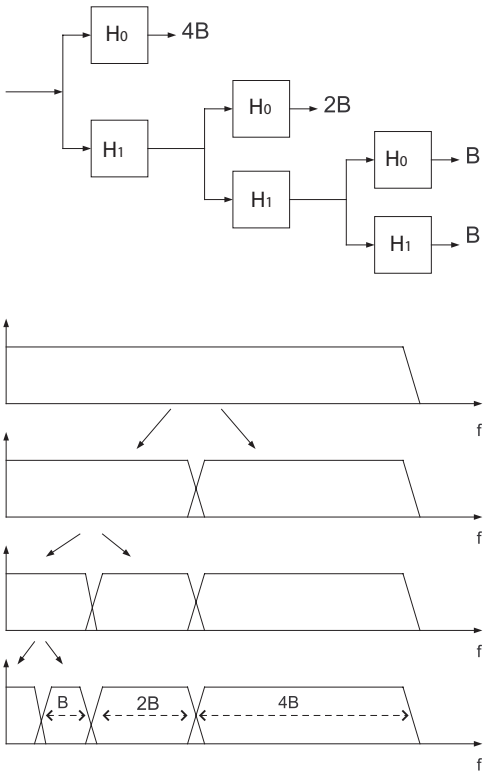

Fig. 1. Wavelet decomposition levels and subband decoding

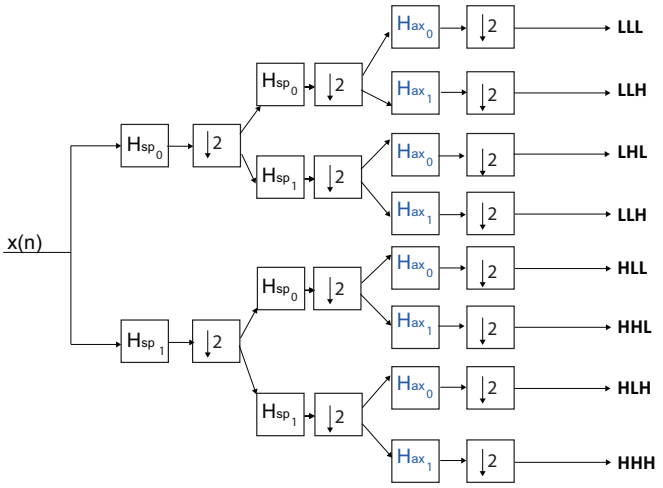

Fig. 2. Non-uniform 3-D wavelet transform

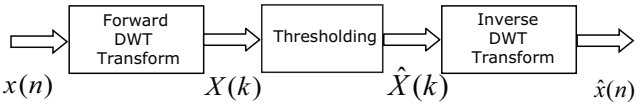

Fig. 3. Ultrasonic compression

information from the original signal and it provides a compact representation.

III. Three Dimensional Wavelet Transform

In 3-D ultrasonic data compression, a set of slices is grouped into one 3-D block and 3-D DWT is applied to the block data to remove inter-slice redundancy. The multiresolution decomposition results in multiple frequency subbands with varying energy content. Most of the energy is concentrated on the lower frequency subband (LLL) which is the convolution outcome of low-pass filters only.

The implementation of the 3-D DWT is very similar to 1-D wavelet transform using filterbanks. The extra implementation steps are the additional filtering operations applied in each coordinate. Fig. 2 shows the block diagram of the non-uniform 3-D wavelet decomposition where the same set of wavelet filters (low pass filter H_{sp_0} and high pass filter H_{sp_1}) are used for the spatial resolutions and a separate wavelet kernel (low pass filter H_{ax_0} and high pass filter H_{ax_1}) is used for the axial resolution. Subbands LLL and HHH represent lowest and highest frequency subbands of the original signal respectively. Since the number of filter operations are significantly higher in the 3-D transform operations, it is imperative to reduce the computations by employing small wavelet filters such as Haar in the spatial resolutions. Haar can be implemented with integer operations, and it requires fewer filtering steps compared to other wavelets.

In order to characterize the compression performance and find the best matching wavelet kernel, multiple wavelet kernels have been utilized for the axial resolution. These wavelets and their coefficients are listed in Table I.

IV. Compression and Thresholding

The data compression of a given signal $x(n)$ is successful when the redundant and noise components of $x(n)$ are reduced or removed. Fig. 3 shows the ultrasonic data compression steps. The signal $\hat{x}(n)$ is the compressed representation of $x(n)$. Thresholding can be applied to transform coefficients of the original ultrasonic signal for data compression. In hard thresholding method, all coefficients smaller than τ are set to zero. All coefficients greater than τ are kept same.

$$X(k) = \begin{cases} 0, & X(k) < \tau \\ X(k), & X(k) \geq \tau \end{cases} \quad (2)$$

A. Thresholding

Two thresholding techniques are used:

1) Determine the threshold using only the LLL subband: Iteratively find a threshold τ for the low frequency subband (LLL) which will preserve a certain amount of its energy. Once τ is calculated, retain all the coefficients above τ and zero all the others. For the high frequency subbands, use the same threshold.
2) Different thresholds in each subband: Calculate energy in each subband prior to quantization. The threshold is calculated such that same amount of energy is retained in each subband. Threshold varies with each subband and is not a constant. Consequently, low frequency subband having maximum energy has the highest threshold where as pure high frequency component has the lowest threshold.

TABLE I
WAVELET KERNEL COEFFICIENTS

Haar		Daubechies 4		Biorthogonal 2.2		Biorthogonal 4.4	
H_0	H_1	H_0	H_1	H_0	H_1	H_0	H_1
		-0.010	-0.230			0.037	-0.064
		0.032	0.714	0	0	-0.023	0.040
		0.030	-0.630	-0.176	0.353	-0.110	0.418
		-0.187	-0.028	0.353	-0.707	0.377	-0.788
0.707	-0.707	-0.028	0.187	1.060	0.353	0.852	0.418
0.707	-0.707	0.630	0.030	0.353	0	0.377	0.040
		0.714	-0.032	-0.176	0	-0.110	-0.064
		0.230	-0.010			-0.023	0
						0.037	0

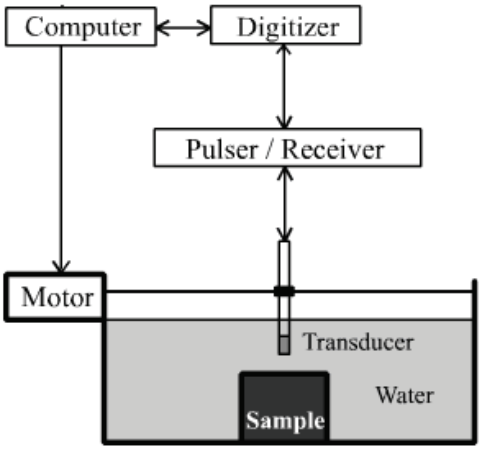

Fig. 4. Ultrasonic experimentation setup

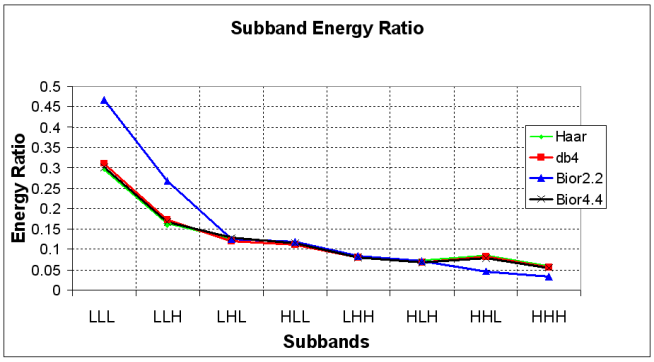

Fig. 5. Energy ratio results for subbands

B. Experimental Setup

A block diagram illustrating ultrasonic data acquisition set up in laboratory is shown in Fig. 4. Experimental setup in laboratory includes a water tank with two step motors mounted on it. A 5 MHz ultrasonic transducer, a pulser/receiver Model 5052 PR, and an HP 54616C oscilloscope are used to acquire, digitize and display the received echo. Two types of data sets are used for the analysis of results. One data set (64*64*256) was generated using steel point source; another data set (60*60*600) was generated using a metal coin.

V. RESULTS

Fig. 5 shows the energy contents of individual subbands with respect to the total energy for multiple wavelet kernels after the transform operation. Biorthogonal 2.2 wavelet provides the most compact representation with 45% of the total energy in a single subband (LLL).

For compression performance analysis, we look at the compression ratio and PSNR values for the non-uniform 3-D wavelet transform using two thresholding techniques. In all cases, Haar wavelet has been used for the spatial resolution while the wavelet kernel for the axial resolution varies.

The compression ratio (CR) is defined as:

$$CR = 1 - \frac{Total\ Points\ after\ compression - zeros}{Total\ Data\ Points - zeros} \quad (3)$$

Zero valued data points are eliminated from the compression ratio calculations in order to reduce the sparseness of the volumetric data. The PSNR is calculated as follows:

$$PSNR = 20log_{10}\left(\frac{Max}{\sqrt{MSE}}\right) \quad (4)$$

where Max is the maximum value of the data set and MSE is the mean square error.

Fig. 6(a) shows the compression results using a threshold determined only with the LLL subband. The best compression ratio is achieved by the Biorthogonal 2.2 wavelet kernel. Biorthogonal 2.2 reduces the data by half while keeping the PSNR at 48dB. This result is consistent with the energy ratio results as shown in Fig. 5 previously.

Fig. 7(a) shows the compression results using separate thresholds in each subband instead of using LLL subband only. For all wavelet kernels, the results show significant improvements for the compression ratios. Biorthogonal 2.2 reduces the data size by a factor of 5 and once again has the best compression performance. Fig. 8 shows the compression ratios for different PSNR values with this thresholding technique.

In order to justify the use of 3-D wavelet transform for volumetric data compression, we compare it with 2-D transform method. In 2-D method, 2-D DWT is applied the

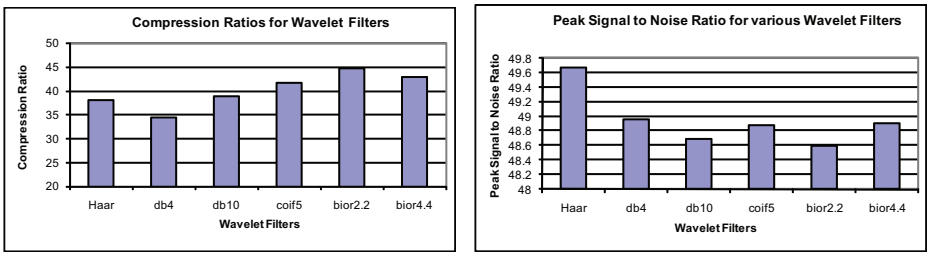

(a) Compression ratio (b) PSNR values

Fig. 6. Non-uniform 3-D DWT compression performance when the threshold is determined by LLL subband

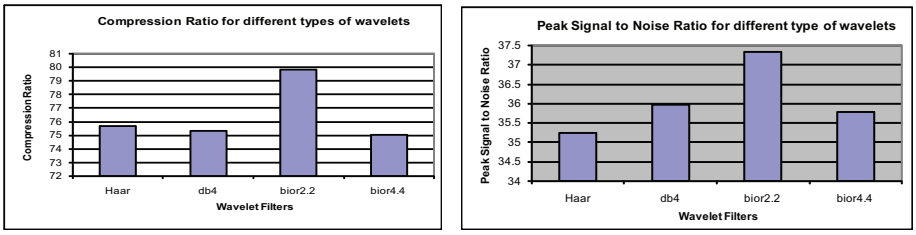

(a) Compression ratio (b) PSNR values

Fig. 7. Non-uniform 3-D DWT compression performance when each subband uses a different threshold

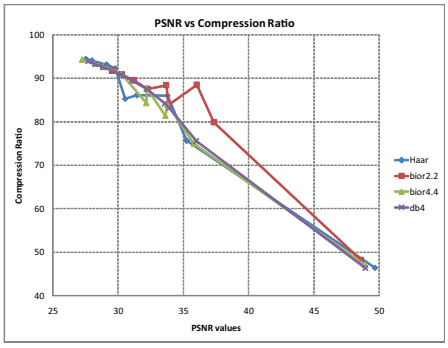

Fig. 8. PSNR versus compression ratio results

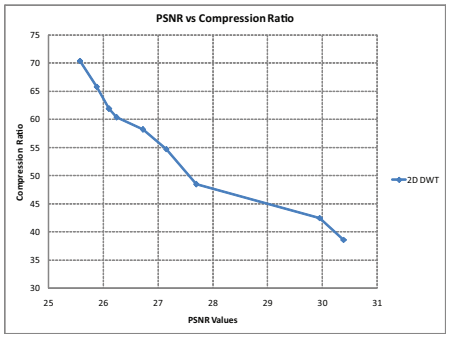

Fig. 9. 2-D DWT compression performance with Bior2.2 wavelet

individual image slices. The total computation is significantly less; however inter-slice redundancy is not exploited. Fig. 9 shows the compression and PSNR values for different wavelet transforms applied to individual slices. The results show a large drop in PSNR values for the same compression ratios.

VI. Conclusion

In this study, we have analyzed DWT based techniques for 3-D ultrasonic data compression. Using non-uniform DWT provides more flexible wavelet kernel choices for spatial and axial resolutions. This can be advantageous especially for reducing the computational complexity of the 3-D transform by using simple wavelet filters such as Haar for the spatial resolution. Therefore, non-uniform DWT is a good candidate for hardware implementation of 3-D wavelet transform with fewer hardware resources and faster throughput.

References

[1] J. M. Shapiro, "Embedded image coding using zerotrees of wavelet coefficients," *IEEE Trans. Signal Process.*, vol. 41, pp. 3445–3462, December 1993.

[2] A. Said and W. Pearlman, "A new fast and efficient coder based on set partitioning in hierarchical trees," *IEEE Trans. Circuits Syst. Video Technol.*, pp. 243–250, June 1996.

[3] D. Taubman and M. Marcellin, *JPEG2000: Image Compression Fundamentals, Standards, and Practice*. Kluwer Academic Publishers, 2001.

[4] G. Cardoso and J. Saniie, "Optimal wavelet estimation for data compression and noise suppression of ultrasonic NDE signals," in *Proc. of the IEEE Ultrasonics Symposium*, vol. 1, Atlanta, Georgia, October 2001, pp. 675–678.

[5] ——, "Ultrasonic data compression via parameter estimation," *IEEE Trans. Ultrason., Ferroelectr., Freq. Control*, vol. 52, pp. 313–325, February 2005.

[6] ——, "Performance evaluation of DWT, DCT, and WHT for compression of ultrasonic signals," in *Proc. of the IEEE Ultrasonics Symposium*, vol. 3, Montreal, Canada, August 2004, pp. 2314–2317.

[7] X. Li, G. Hu, and S. Gao, "Design and implementation of a novel compression method in a tele ultrasound system," *IEEE Trans. Inf. Technol. Biomed.*, vol. 3, pp. 205–213, September 1999.

[8] J. Wang and H. K. Huang, "Medical image compression by using three-dimensional wavelet transformation," *IEEE Trans. Biomed. Eng.*, vol. 15, pp. 547–554, August 1996.